



Hydrogen production through oxidative steam reforming of ethanol over Ni-based catalysts derived from $\text{La}_{1-x}\text{Ce}_x\text{NiO}_3$ perovskite-type oxides

Sania M. de Lima^{a,b}, Adriana M. da Silva^b, Lídia O.O. da Costa^b, José M. Assaf^c, Lisiâne V. Mattos^d, Reema Sarkari^e, A. Venugopal^e, Fábio B. Noronha^{b,*}

^a Universidade Federal de São Paulo – UNIFESP, Departamento de Ciências Exatas e da Terra – Setor de Engenharia Química, Rua Prof. Artur Riedel, 275 – Jd. Eldorado, CEP 09972-270, Diadema, Brazil

^b Instituto Nacional de Tecnologia – INT, Av. Venezuela 82, CEP 20081-312, Rio de Janeiro, Brazil

^c Universidade Federal de São Carlos – UFSCar, Laboratório de Catálise, Via Washington Luiz, Km 235, CEP 13565-905, São Carlos, Brazil

^d Universidade Federal Fluminense, Rua Passo da Pátria, 156, Niterói, RJ CEP 24210-240, Brazil

^e Inorganic and Physical Chemistry Division, Indian Institute of Chemical Technology, Hyderabad 500607, India

ARTICLE INFO

Article history:

Received 17 October 2011

Received in revised form 7 March 2012

Accepted 15 March 2012

Available online 26 March 2012

Keywords:

Perovskite-type oxides

Hydrogen production

Ethanol oxidative steam reforming

Deactivation mechanism

Nickel catalyst

ABSTRACT

This paper investigates the effect of lanthanum substitution by cerium oxide on the performance of $\text{La}_{1-x}\text{Ce}_x\text{NiO}_3$ ($x=0, 0.05, 0.1, 0.4, 0.7$ and 1.0) perovskite-type oxide precursor for the oxidative steam reforming of ethanol. All catalysts are active and selective to hydrogen but carbon deposition occurs except for $\text{La}_{0.90}\text{Ce}_{0.10}\text{NiO}_3$. Increasing the Ce content decreases the amount of carbon deposited, which passes through a minimum at around 10 wt% of Ce and then increases. The higher resistance to carbon formation on $\text{La}_{0.90}\text{Ce}_{0.10}\text{NiO}_3$ catalyst is due to the smaller Ni crystallite size. Furthermore, the support also plays an important role on catalyst stability during ethanol conversion reaction. The reduced $\text{La}_{0.9}\text{Ce}_{0.1}\text{NiO}_3$ sample exhibits the highest amount of oxygen vacancies, which decreases as ceria content increases. This highly mobile oxygen reacts with carbon species as soon as it forms, and thus keeps the metal surface free of carbon, inhibiting deactivation.

© 2012 Elsevier B.V. All rights reserved.

1. Introduction

Hydrogen production through ethanol conversion reactions has been extensively studied in the literature [1–4]. The main challenge is the development of a catalyst that is active, selective to hydrogen and stable under reaction conditions. In the search for this catalyst, different metal oxides [5,6], supported base metals (Ni, Co, Cu) [7–10] and noble metals (Pd, Pt, Rh, Ru) [11–14] have been tested for steam reforming (SR), partial oxidation (POX) and oxidative steam reforming (OSR) of ethanol. Regardless of the metal and support used, significant deactivation has been reported in the open literature over Ru [11], Pt [15], Pd [16], Rh [17], Ir [18], Co [19], and Ni [20] based catalysts. Catalyst deactivation is generally attributed to the deposition of carbonaceous species and the sintering of metal particles. Therefore, the design of a catalyst resistant to coke formation and metal sintering is still an issue.

The perovskite-type oxide with general formula ABO_3 is a promising material as catalyst for the ethanol conversion reactions to hydrogen. These mixed oxides are able to produce highly

dispersed metallic particles upon reduction, which inhibit the formation of carbon [21]. Furthermore, the perovskite-type oxide exhibits a high oxygen mobility, which may be beneficial for the removal of carbon deposits [9,22]. However, there are only few studies about perovskites employed as catalyst precursor for the steam reforming of ethanol [23–28].

Recently, we have studied the performance of LaNiO_3 perovskite-type oxide precursor as a catalyst for both SR and OSR of ethanol [28]. Catalyst deactivation took place depending on the reaction conditions and it is attributed to the deposition of carbon on the surface of the catalyst. Both thermogravimetric (TG) and scanning electron microscopy (SEM) analyses of post-reaction samples showed that lower reaction temperatures and lower $\text{H}_2\text{O}/\text{EtOH}$ ratios favored the deposition of filamentous carbon. However, less carbon formation occurs when the $\text{H}_2\text{O}/\text{EtOH}$ ratio is increased. Increasing reaction temperature suppressed carbon formation whereas the addition of oxygen to the feed significantly reduced carbon deposits.

Partial substitution of cations in positions A and B while preserving the perovskite structure, induces important changes in its properties. For instance, the thermal stability of perovskites depends on the cations at positions A and B. Partial substitution of the A ion by another one at a lower oxidation state may: (i)

* Corresponding author. Tel.: +55 21 2123 1177; fax: +55 21 2123 1166.

E-mail address: fabio.bellot@int.gov.br (F.B. Noronha).

affect thermal stability under reducing atmosphere; (ii) increase the mobility of oxygen ion vacancies. The reduction properties of the perovskite-type oxide are directly correlated to the catalytic activity of these materials for oxidation reactions [29]. In addition, the incorporation of a low valence cation in the A-site decreases the valence that is compensated by the creation of oxygen vacancies. The literature reports that the higher reducibility and oxygen storage/release capacity of perovskite-type oxides catalysts may promote the mechanism of continuous removal of carbonaceous deposits from the active sites in reactions like partial oxidation and the CO₂ reforming (i.e., dry reforming) of methane [29,30].

In particular, the substitution at the A-site in perovskites like La_{1-x}Ce_xNiO₃ improved the activity of methane combustion [31]. Mixed oxides La_{1-x}Ce_xNiO₃ ($x=0, 0.05, 0.4$ and 0.7) have been tested in the CO₂ reforming of methane reaction into synthesis gas [30]. The LaNiO₃ perovskite is active in the methane reforming, but underwent a slow deactivation with time-on-stream (TOS). Nevertheless, substitution of the A site metal ion with a tetravalent metal cation (Ce⁴⁺) increased the catalytic activity. In addition, the insertion of Ce improved the stability of the catalysts during the reforming reaction.

The aim of this work is to study the effect of substitution of La³⁺ by Ce³⁺ in the performance of reduced La_{1-x}Ce_xNiO₃ perovskite-type oxides for the OSR of ethanol. The incorporation of ceria into the perovskite structure is evaluated in terms of catalyst stability and the amount and nature of carbon formed is investigated by transmission electron microscopy (TEM) and TG analysis.

2. Experimental

2.1. Catalyst preparation

Substituted La_{1-x}Ce_xNiO₃ ($x=0, 0.05, 0.1, 0.4, 0.7$ and 1.0) perovskites were prepared by amorphous citrate decomposition as described earlier [30]. Aqueous solutions of La(NO₃)₃·5H₂O (Aldrich), Ce(NO₃)₃·6H₂O (Aldrich), Ni(NO₃)₂·6H₂O (Aldrich) in appropriate quantities to give perovskites with the desired formula were prepared and mixed. Thus, a concentrated solution of citric acid was prepared and then added to the solution of the metal nitrates, in such a way that the ratio of equivalent grams of metal to equivalent grams of citric acid would be unity, to form the metallic amorphous citrates. The resulting solution was evaporated to dryness at 383 K for 48 h, which resulted in a spongy material. This citrate precursor obtained was then crushed and calcined in two stages; first at 823 K for 3 h and then at 1173 K for 10 h, to obtain the final perovskite structure. Although pure perovskite oxide is not formed along the series, and in some cases this structure is not present ($x=0.7$ and 1.0), the nomenclature La_{1-x}Ce_xNiO₃ has been used in all cases just for uniformity as a general practice seen in the literature [29].

2.2. BET surface area

The BET surface areas of the samples were measured using a Quantachrome NOVA 1200 instrument by nitrogen adsorption at the boiling temperature of liquid nitrogen.

2.3. X-ray diffraction (XRD)

The X-ray powder diffraction pattern of the calcined and reduced/passivated samples was obtained with nickel-filtered CuK α radiation ($\lambda=1.5418\text{ \AA}$) using a Siemens D5005 diffractometer. The XRD data were collected between $2\theta=5$ and 80° (in steps of $2^\circ/\text{min}$). The sample was reduced with H₂ (30 mL/min) at 973 K/1 h,

cooled to room temperature, and passivated with 4.5% O₂/He mixture.

2.4. Temperature-programmed reduction (TPR)

TPR experiments were carried out on a Micromeritics TPD/TPR 2900 apparatus. The sample (30 mg) was pretreated at 773 K for 1 h under a flow of air (50 mL/min) prior to the TPR experiment in order to remove traces of water. Reduction profiles were then recorded by passing a stream of 10% H₂/Ar at a flow rate of 50 mL/min, while heating the sample at a rate of 10 K/min from ambient temperature to 1173 K. A cold-trap was placed just before the thermal conductivity detector (TCD) of the instrument to remove the water from the exit stream.

2.5. Oxygen storage capacity (OSC)

Oxygen storage capacity measurements were carried out using a multipurpose unit connected to a quadrupole mass spectrometer (Balzers, Omnistar). Each sample (100 mg) was reduced under flowing H₂ at 1023 K for 1 h. Then, it was cooled to 723 K and a 5% O₂/He mixture was passed through the catalyst until uptake of oxygen reached saturation. The reactor was purged with He and the dead volume was obtained by switching the gas to the 5%O₂/He mixture. Finally the amount of oxygen consumed by the catalyst was calculated by injecting pulses of O₂.

2.6. TG analysis

Temperature programmed oxidation (TPO) experiments were performed using a TA Instrument TGA analyzer (SDT Q600) in order to quantify the amount of carbon formed over the catalyst. Approximately 10 mg of spent catalyst was heated under air flow from room temperature to 1173 K at a heating rate of 20 K/min and the corresponding change in weight was measured.

2.7. TEM

The transmission electron microscope analyses of the used catalysts were performed using JEOL JEM 2010 high-resolution transmission electron microscope. The samples were dispersed in methanol solution and suspended on a 400-mesh, 3.5 mm diameter Cu grid.

2.8. Scanning electron microscopy

Scanning electron microscopy analyses of the spent catalysts was carried out using a FEI Inspect S scanning electron microscope equipped with a secondary electron analyzer. The microscope was also equipped with an EDAX analytic system energy dispersive spectrometer (EDS).

2.9. Reaction conditions

OSR of ethanol was performed in a quartz tube (4 mm inner diameter) reactor at atmospheric pressure. Prior to reaction, catalysts were reduced under pure H₂ (30 mL/min) at 973 K for 1 h and then purged with N₂ at the same temperature for 30 min. All reactions were carried out at 773 K. OSR was performed employing a H₂O/ethanol molar ratio of 3.0 and an O₂/ethanol molar ratio of 0.5 (2.5% ethanol; 7.5% water, 1.25% oxygen; 88.75% nitrogen). The reactant mixtures were obtained using two saturators containing water and ethanol, which were maintained at the temperature required to obtain the desired H₂O/ethanol and O₂/ethanol molar ratios. A flow of 5.6 mol% O₂ in N₂ (28 mL/min) and a flow of N₂

Table 1

BET surface area, Ni⁰ crystallite size obtained by XRD and amount of carbon deposited on La_{1-x}Ce_xNiO₃ catalyst after OSR of ethanol, as determined by TGA, using 5%O₂/He and a heating rate of 10 K/min.

Samples	Surface area (m ² /g)	d (nm)	mg C/g _{cat} /h
LaNiO ₃	1.1	21.5	1.4
La _{0.95} Ce _{0.05} NiO ₃	0.6	19.8 (21.2) ^a	1.0
La _{0.90} Ce _{0.10} NiO ₃	2.4	16.5	0.0
La _{0.60} Ce _{0.40} NiO ₃	0.2	22.6	3.9
La _{0.30} Ce _{0.70} NiO ₃	0.2	26.8	16.8
CeNiO ₃	–	30.5 (109.2) ^a	23.0

^a Ni⁰ crystallite size determined by TEM of used catalysts.

(32 mL/min) were passed through the saturators containing water and ethanol, respectively.

In order to observe the deactivation of the catalyst within a short period of time, a small amount of catalyst was used (20 mg), which corresponded to a residence time of $W/Q = 0.02 \text{ g s/mL}$ (W = weight of catalyst; Q = volumetric flow rate). The samples were diluted with inert SiC (SiC mass/catalyst mass=3.0) with the catalyst bed height being around 3 mm. The reaction products were analyzed by gas chromatography (Micro GC Agilent 3000 A containing three channels for triple thermal conductivity detectors and three columns: a molecular sieve, a plot-Q and an OV-1 column). The ethanol conversion and selectivity to products were determined from:

$$X_{\text{ethanol}} = \frac{(n_{\text{ethanol}})_{\text{fed}} - (n_{\text{ethanol}})_{\text{exit}}}{(n_{\text{ethanol}})_{\text{fed}}} \times 100 \quad (1)$$

$$S_x = \frac{(n_x)_{\text{produced}}}{(n_{\text{total}})_{\text{produced}}} \times 100 \quad (2)$$

where $(n_x)_{\text{produced}}$ = moles of x produced (x =hydrogen, CO, CO₂, methane, acetaldehyde or ethene) and $(n_{\text{total}})_{\text{produced}}$ = moles of H₂ + moles of CO + moles of CO₂ + moles of methane + moles of acetaldehyde + moles of ethene (the moles of water produced are not included).

3. Results and discussion

3.1. Catalyst characterization

The BET surface area of all perovskite-type oxides is very low (<10.0 m²/g) (Table 1), which is characteristic of these materials prepared after calcination at high temperature.

The XRD patterns of the calcined samples are displayed in Fig. 1. The diffraction lines at $2\theta = 23.35, 32.98, 47.37$ and 58.66° are characteristic of the LaNiO₃ rhombohedral phase (JCPDF 330711) [30], indicating that the perovskite structure is the main phase obtained after calcination for the Ce-free oxide ($x=0$).

The substitution of La by 5% of Ce resulted in the appearance of the most intense diffraction line of La₂NiO₄ ($2\theta = 32.48^\circ$) phase together with the lines of LaNiO₃ perovskite ($2\theta = 23.29, 32.99, 47.41$ and 58.51°). The La_{0.9}Ce_{0.1}NiO₃ precursor exhibited basically the lines associated with perovskite structure ($2\theta = 32.99, 47.29$ and 58.63°). Increasing the concentration of Ce drastically decreased the intensity of the lines attributed to the perovskite phase, which is no longer detected for the La_{0.3}Ce_{0.7}NiO₃ precursor. In addition, the appearance of new phases assigned to NiO ($2\theta = 37.27, 43.27$ and 62.91°) and CeO₂ ($2\theta = 28.60, 33.13, 47.52, 56.39$ and 76.73°) with cubic structure for La_{1-x}Ce_xNiO₃ precursors with $x=0.4, 0.7$ and 1.0 , are also observed.

For the La_{1-x}Ce_xNiO₃ precursors with $x=0.05$ and 0.1 , there was no shift in the lines characteristic of LaNiO₃ perovskite. This is expected since the ionic radius of La³⁺ and Ce³⁺ ions is very close (1.17 and 1.15 Å, respectively). In addition, there are no lines related to CeO₂ phase. Therefore, these results suggest that La³⁺ was

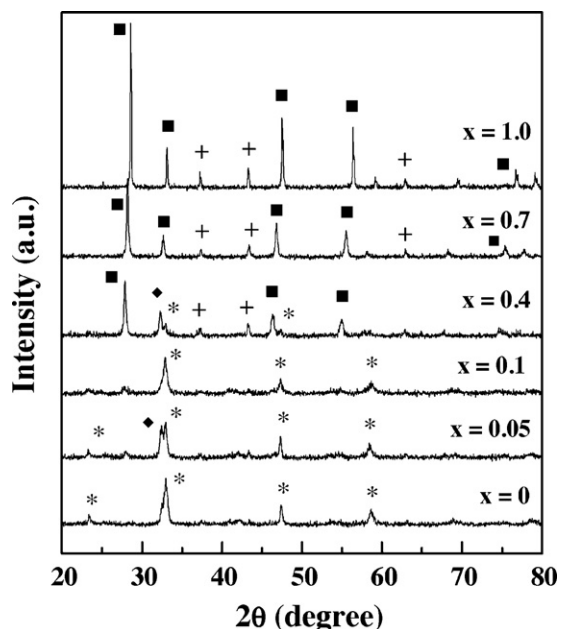


Fig. 1. XRD patterns of La_{1-x}Ce_xNiO₃ perovskite oxides. (*) LaNiO₃ perovskite, (■) CeO₂, (+) NiO, (◆) La₂NiO₄.

partially substituted by Ce³⁺ in the perovskite structure. Increasing the cerium content ($x \geq 0.4$), the decrease of the intensity of the lines typical of LaNiO₃ perovskite and the appearance of the lines corresponding to the NiO and CeO₂ phases suggests that the saturation point of cerium doping was achieved at $x=0.4$. These results are in agreement with the studies involving La_{1-x}Ce_xNiO₃ and La_{1-x}Ce_xCoO₃ perovskites in the literature [30,32]. XPS analysis revealed the presence of a higher fraction of Ce³⁺ ions in the La_{1-x}Ce_xNiO₃ precursor with $x=0.05$, indicating that cerium was incorporated into the perovskite structure [30]. For the samples containing $x \geq 0.4$, XPS results suggested that cerium is essentially in the Ce⁴⁺ oxidation state, leading to the segregation of CeO₂. For La_{1-x}Ce_xCoO₃ perovskites, it was reported a limit for Ce segregation between 5% and 10% [32]. The partial substitution of La³⁺ with Ce⁴⁺ resulted in the conversion of Co³⁺ to Co²⁺ in order to keep the charge neutrality. Since the ionic radius of Co²⁺ is larger than that of Co³⁺, this leads to a decrease of the tolerance factor and consequently to the segregation of Ce.

The reduction profile of LaNiO₃ perovskite-type oxide exhibited a broad peak with a maximum at 660 K and a shoulder at around 600 K and a second peak at 776 K (Fig. 2). Recently, we have studied the transformations occurring during the reduction of a LaNiO₃ perovskite-type oxide prepared by the precipitation method [28]. The TPR profile exhibited three peaks at 614, 640 and 770 K. The reduction peak at 614 K was attributed to the reduction of Ni³⁺ to Ni²⁺, and the peak at 770 K was due to the reduction of Ni²⁺ to Ni⁰, both coming from the perovskite structure. This result also revealed that the reduction treatment at 973 K destroyed the perovskite structure and Ni⁰ particles are deposited over lanthanum oxide. The intermediate peak at around 640 K is associated with the reduction of Ni²⁺ (of a nickel oxide phase) to Ni⁰. Therefore, in the present work, the TPR profile of LaNiO₃ precursor prepared by citrate method showed the presence of LaNiO₃ perovskite (600 and 776 K) and NiO (660 K). The reduction profile of La_{0.95}Ce_{0.05}NiO₃ and La_{0.9}Ce_{0.1}NiO₃ precursors are very similar to the one observed for LaNiO₃, with a shoulder at 600 K, which is more defined for the La_{0.9}Ce_{0.1}NiO₃ precursor.

The TPR profiles of La_{1-x}Ce_xNiO₃ precursors significantly changed for $x \geq 0.4$. The intensity of the first peak (650–671 K)

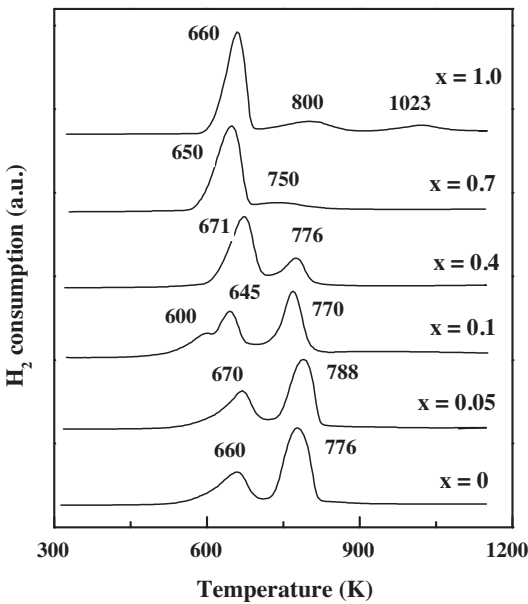


Fig. 2. TPR profiles of $\text{La}_{1-x}\text{Ce}_x\text{NiO}_3$ perovskite oxides.

is found to be much higher than the second one (750–776 K), which disappeared on CeNiO_3 sample. Increasing Ce concentration, XRD pattern showed that NiO and CeO_2 are the main phases present while LaNiO_3 perovskite structure is no longer detected for $\text{La}_{1-x}\text{Ce}_x\text{NiO}_3$ precursors with $x = 0.7$ and 1.0 . Therefore, the first peak corresponds mainly to the reduction of Ni^{2+} to Ni^0 from NiO whereas the reduction in two steps of Ni^{3+} to Ni^0 from the perovskite structure occurs in a limited extent for $x = 0.4$. For CeNiO_3 , the peaks at 800 and 1023 K are due to surface and bulk reduction of CeO_2 , respectively [33].

The diffractograms of the $\text{La}_{1-x}\text{Ce}_x\text{NiO}_3$ precursors after reduction at 973 K and passivation are shown in Fig. 3. The diffractogram of reduced LaNiO_3 revealed the presence of lines typical of La_2O_3

($2\theta = 26.0, 29.9, 39.3, 46.0, 52.0, 55.7, 62.1^\circ$) and Ni^0 ($2\theta = 44.4, 52.0^\circ$), indicating that the perovskite structure is destroyed during reduction [28]. The reduced $\text{La}_{0.95}\text{Ce}_{0.05}\text{NiO}_3$ exhibited basically the same lines observed for LaNiO_3 sample except for the weak line at $2\theta = 27.8^\circ$ that is characteristic of La(OH)_3 . For the reduced $\text{La}_{0.9}\text{Ce}_{0.1}\text{NiO}_3$ sample, the intensity of the lines typical of La_2O_3 were significantly decreased and the diffractogram is dominated by the lines corresponding to the La(OH)_3 phase ($2\theta = 15.7, 28.0, 39.6, 48.7^\circ$). It is also noticed the presence of lines at $2\theta = 27.3$ and 31.7° , which may be attributed to the CeO_3 phase [34]. Increasing ceria content, the intensity of these lines increased and they were shifted to higher angles. For instance, the diffractogram of reduced $\text{La}_{0.60}\text{Ce}_{0.40}\text{NiO}_3$ exhibited lines at $2\theta = 27.7, 32.2, 46.2, 54.7, 57.5, 67.4, 74.4^\circ$ that corresponds to the $\text{CeO}_{1.698}$ phase [35]. For CeNiO_3 , the lines at $2\theta = 28.6, 33.1, 47.4, 56.3, 59.2, 69.5, 76.7, 79.0^\circ$ are characteristic of CeO_2 structure [33]. Therefore, these results revealed the presence of a higher amount of oxygen vacancies on the reduced $\text{La}_{0.9}\text{Ce}_{0.1}\text{NiO}_3$ sample, which decreased as ceria content increased. In addition, all catalysts containing ceria exhibited the lines characteristic of Ni^0 ($2\theta = 44.4, 52.0^\circ$), which became more intense and sharper as the ceria content increased. In order to confirm these results, OSC measurements were carried out for $\text{La}_{0.9}\text{Ce}_{0.1}\text{NiO}_3$ and CeNiO_3 samples. The oxygen storage capacity of the reduced $\text{La}_{0.9}\text{Ce}_{0.1}\text{NiO}_3$ sample (1443 $\mu\text{mol O}_2/\text{gcat}$) was considerably higher than that of the reduced CeNiO_3 sample (544 $\mu\text{mol O}_2/\text{gcat}$). These results agree very well with the phases detected in the diffractograms of the reduced catalysts, showing a higher concentration of oxygen vacancies for the $\text{La}_{0.9}\text{Ce}_{0.1}\text{NiO}_3$ sample.

From the diffraction line of Ni^0 at $2\theta = 44.9^\circ$, the nickel crystallite size is calculated using the Scherrer equation for the reduced $\text{La}_{1-x}\text{Ce}_x\text{NiO}_3$ samples and the results are listed in Table 1. The Ni crystallite size of reduced LaNiO_3 is 21.5 nm. The addition of 5% and 10% of Ce decreased the nickel crystallite size ($d_p = 19.8$ and 16.5 nm, respectively). Increasing the concentration of Ce to 100% (CeNiO_3) significantly increased the nickel crystallite size (30.5 nm).

3.2. Reaction testing

3.2.1. OSR at 773 K

Fig. 4a–f shows the performance of $\text{La}_{1-x}\text{Ce}_x\text{NiO}_3$ catalysts for the OSR reaction at 773 K. The initial ethanol conversion for OSR is around 100% and only slightly decreased after 5 h, remaining quite constant until 30 h of TOS for all catalysts. Regarding product distribution, H_2 and CO_2 are the main products formed. CO and CH_4 are also detected over all catalysts. Only small amount of acetaldehyde (less than 3%) is formed on $\text{La}_{1-x}\text{Ce}_x\text{NiO}_3$ ($x = 0, 0.05$ and 0.1). Significant formation of acetaldehyde occurred during OSR over $\text{La}_{1-x}\text{Ce}_x\text{NiO}_3$ with $x = 0.4$ and 0.7 . However, there is no clear correlation observed between product distribution and Ce content.

Recently, we have studied the performance of Ni-based catalyst prepared from LaNiO_3 perovskite-type oxide during OSR of ethanol at 773 K. The presence of oxygen in the feed strongly inhibited carbon deposition and significantly improved catalyst stability [28]. Carbon deposition was also significantly suppressed during OSR of ethanol over reduced LaNiO_3 catalyst, which remained quite stable during TOS [27]. Chen et al. [26] investigated the performance of reduced-oxidized $\text{La}_{1-x}\text{Ce}_x\text{Fe}_{0.7}\text{Ni}_{0.3}\text{O}_3$ perovskite-type oxides during OSR of ethanol. The stability of the catalyst was attributed to the presence of oxygen that inhibited the metallic Ni particle growth during reaction. In order to determine the reasons of the stability of our catalysts, we carried out TG and TEM analyses of the post-reaction catalysts.

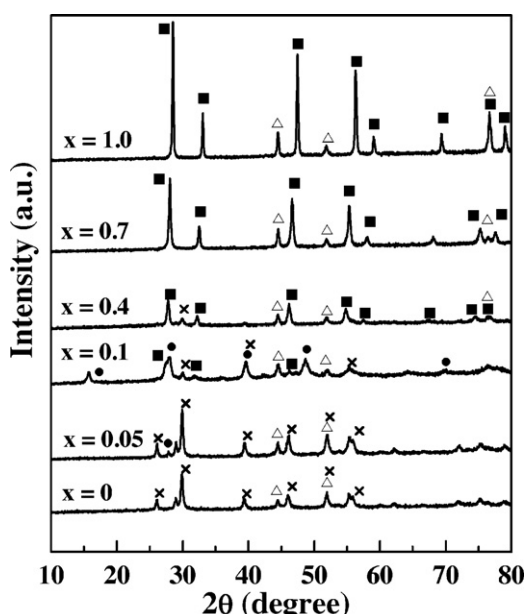


Fig. 3. XRD patterns of reduced and passivated $\text{La}_{1-x}\text{Ce}_x\text{NiO}_3$ samples. (x) La_2O_3 , (●) La(OH)_3 , (△) Ni^0 , (■) CeO_x .

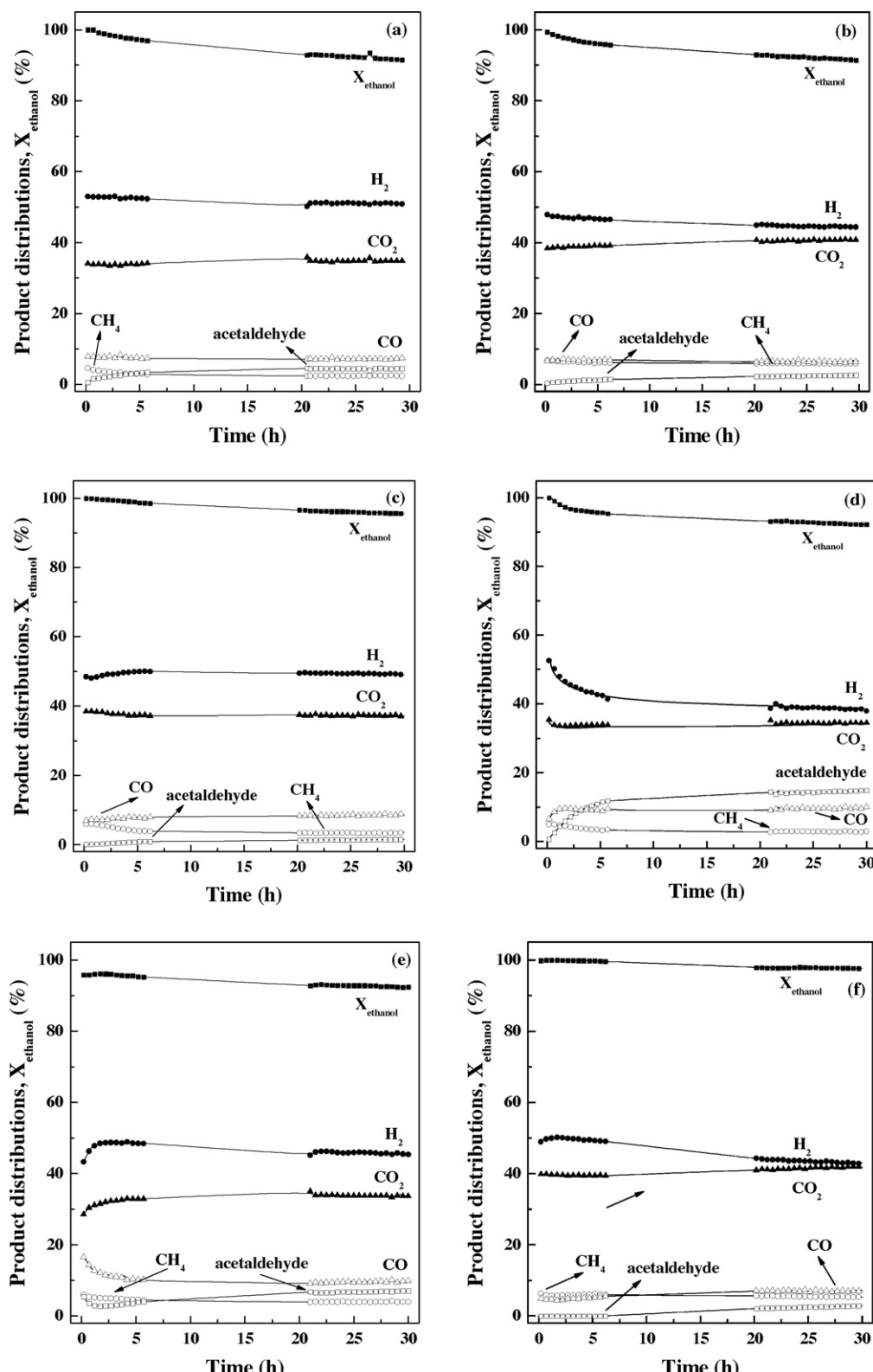


Fig. 4. Ethanol conversion (X_{ethanol}) and product distributions versus time on stream over $\text{La}_{1-x}\text{Ce}_x\text{NiO}_3$ catalysts obtained during OSR under $\text{H}_2\text{O}/\text{ethanol}$ molar ratio = 3.0 and $\text{O}_2/\text{ethanol}$ molar ratio = 0.5 at 773 K over: (a) LaNiO_3 ; (b) $\text{La}_{0.95}\text{Ce}_{0.05}\text{NiO}_3$; (c) $\text{La}_{0.9}\text{Ce}_{0.1}\text{NiO}_3$; (d) $\text{La}_{0.6}\text{Ce}_{0.4}\text{NiO}_3$; (e) $\text{La}_{0.3}\text{Ce}_{0.7}\text{NiO}_3$; (f) CeNiO_3 . (Mass of catalyst = 20 mg and residence time = 0.02 g s/mL.)

3.2.2. Characterization of post-reaction catalysts after OSR at 773 K

The derivatives of mass-loss curves of the $\text{La}_{1-x}\text{Ce}_x\text{NiO}_3$ catalysts after OSR are shown in Fig. 5. The TPO profile of LaNiO_3

exhibited a broad peak at 834 K. Replacing 5% of La by Ce did not change significantly the TPO profile, which showed a peak at 818 K. However, this peak was no longer detected when the catalyst contained 10% of Ce. Further increase in the Ce content led to the

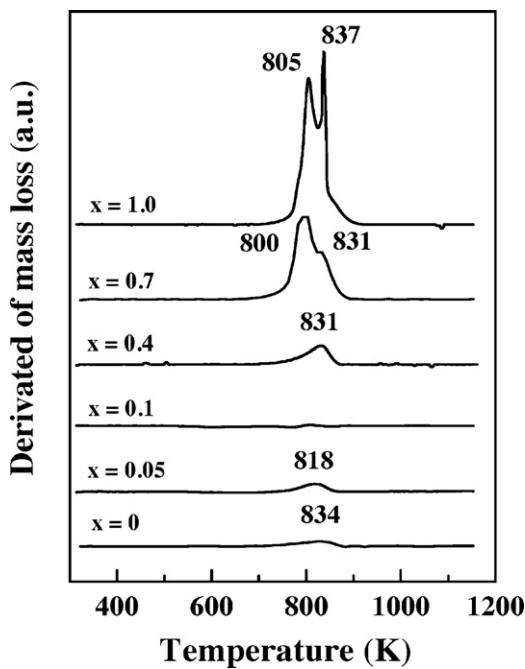


Fig. 5. TPO profile of $\text{La}_{1-x}\text{Ce}_x\text{NiO}_3$ perovskite oxides after OSR of ethanol under $\text{H}_2\text{O}/\text{ethanol}$ molar ratio = 3.0 and $\text{O}_2/\text{ethanol}$ molar ratio = 0.5 at 773 K. (Mass of catalyst = 20 mg and residence time = 0.02 g s/mL.)

appearance of two peaks, the first being around 800–805 K and the second in the range of 831–837 K for $\text{La}_{0.3}\text{Ce}_{0.7}\text{NiO}_3$ and CeNiO_3 spent catalysts, respectively.

The amount of carbon deposited on all catalysts after OSR is listed in Table 1. Increasing the Ce content decreased the amount of carbon deposited, which passed through a minimum at around 10% of Ce and then it rose steadily. The catalyst containing the highest amount of ceria exhibited the highest amount of carbon deposits.

In the literature, the peaks observed during TPO after SR and OSR of ethanol are attributed to the presence of different types of carbon on the surface of the spent catalyst such as: amorphous carbon, filamentous carbon, graphitic carbon, polymeric carbon stemming from ethylene polymerization and CH_x species [5,28,36,37]. The nature and amount of carbon formed depended on both the reaction conditions and catalyst used.

In our previous study, the TPO profiles of the LaNiO_3 catalyst after exposure to different reaction conditions displayed two peaks at around 790–813 K and 830–864 K [28]. The oxidation peaks at low temperatures were attributed to the presence of filamentous carbon (single wall and multi-walled carbon nanotubes). The peak at high temperature was due to oxidation of graphitic carbon. These results agree very well with our present work.

In order to characterize the nature of the carbonaceous species formed over $\text{La}_{1-x}\text{Ce}_x\text{NiO}_3$ catalysts after OSR of ethanol, TEM analysis is carried out and the images are shown in Fig. 6. TEM micrograph of the $\text{La}_{0.95}\text{Ce}_{0.05}\text{NiO}_3$ catalyst shows the presence of few carbon filaments (Fig. 6a). However, a large amount of carbon, in the form of carbon filaments, is clearly observed after OSR over $\text{La}_{0.3}\text{Ce}_{0.7}\text{NiO}_3$ and CeNiO_3 (Fig. 6b and c). These results agree very well with the TPO assignments of carbon species. In addition, it is noticed that Ni particles are located at the ends of carbon filaments. Therefore, the metal remains active during the OSR because the surface remains exposed to the reactants and thus, the carbon formed did not result in significant catalyst deactivation. This can explain the stability of reduced CeNiO_3 catalyst (Fig. 4f) despite having a considerable amount of carbon formed.

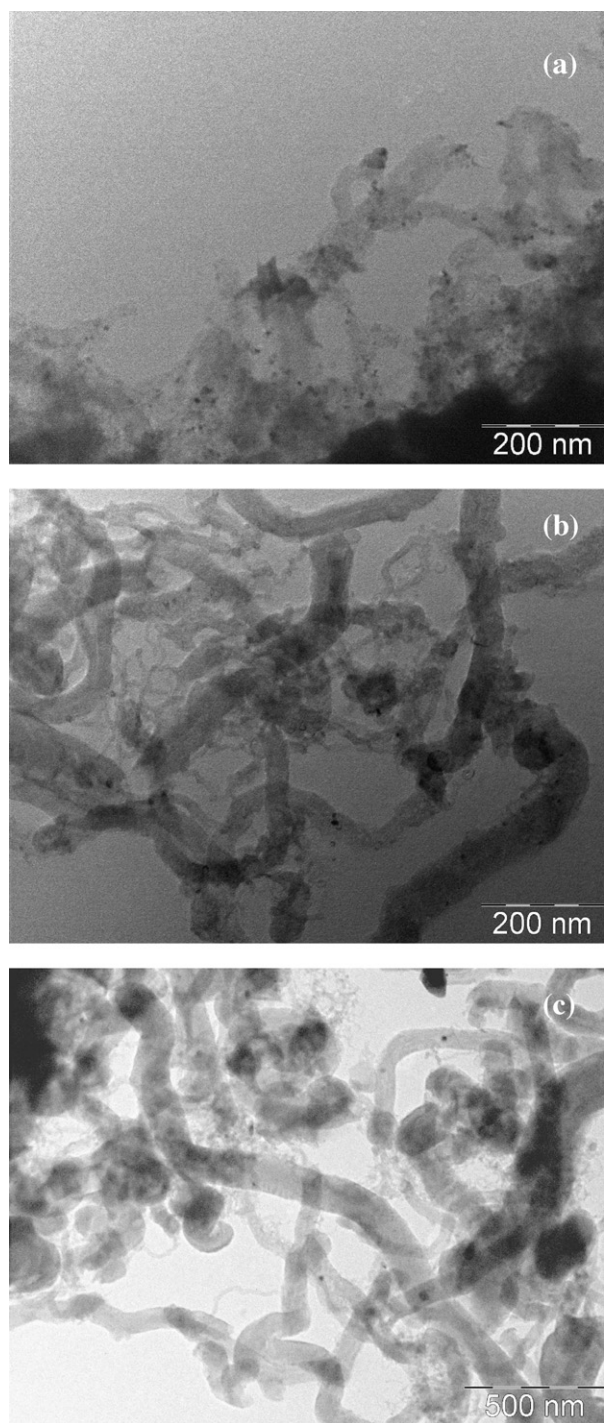


Fig. 6. TEM images after OSR of ethanol under $\text{H}_2\text{O}/\text{ethanol}$ molar ratio = 3.0 and $\text{O}_2/\text{ethanol}$ molar ratio = 0.5 at 773 K: (a) $\text{La}_{0.95}\text{Ce}_{0.05}\text{NiO}_3$; (b) $\text{La}_{0.3}\text{Ce}_{0.7}\text{NiO}_3$; (c) CeNiO_3 . (Mass of catalyst = 20 mg and residence time = 0.02 g s/mL.)

Since the $\text{La}_{0.9}\text{Ce}_{0.1}\text{NiO}_3$ catalyst did not exhibit the formation of carbon during OSR at 773 K, this catalyst was studied in greater detail.

3.2.3. OSR under different reaction conditions over $\text{La}_{0.9}\text{Ce}_{0.1}\text{NiO}_3$ catalyst

Fig. 7a and b shows the performance of $\text{La}_{0.9}\text{Ce}_{0.1}\text{NiO}_3$ catalyst for the OSR reaction at 573 and 1073 K. The ethanol conversion remains constant (28%) during reaction at 573 K. However, the main products were acetaldehyde, CO_2 and small amounts of CH_4

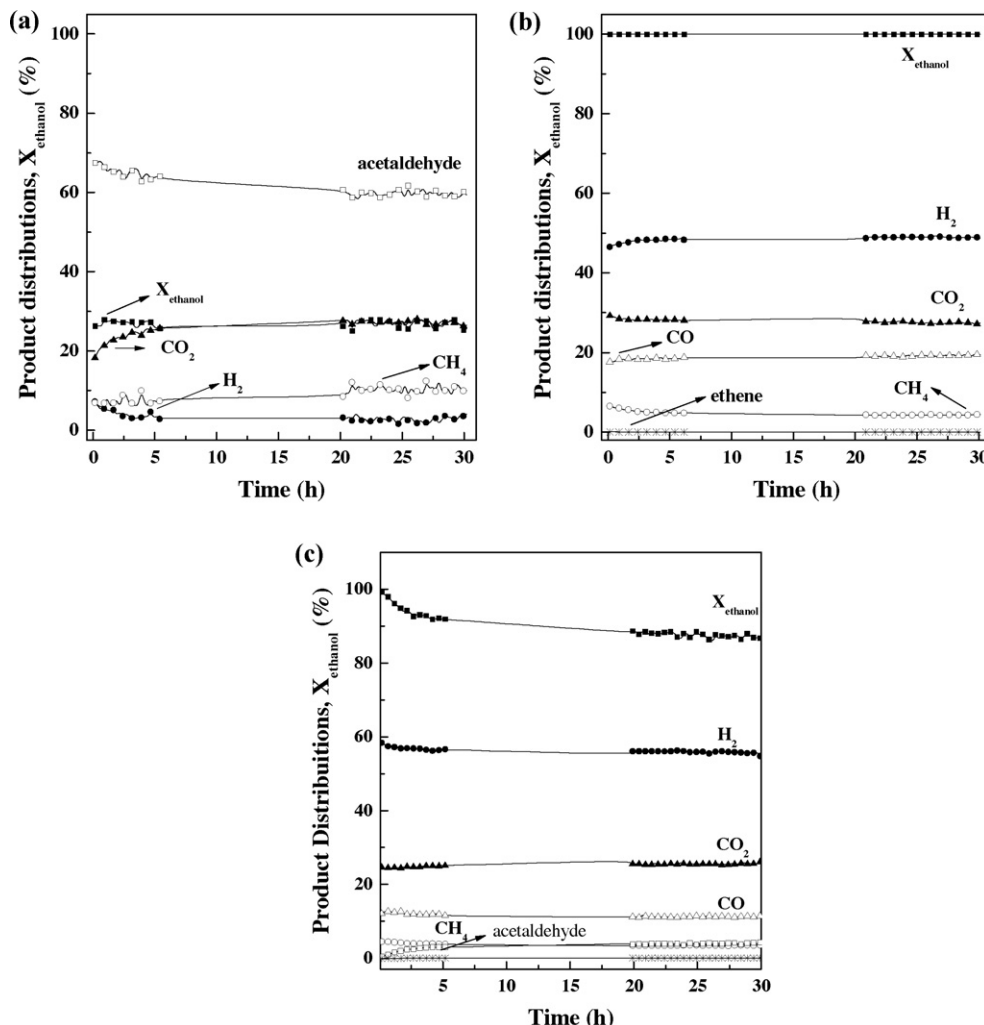


Fig. 7. Ethanol conversion (X_{ethanol}) and product distributions versus time on stream over $\text{La}_{0.90}\text{Ce}_{0.10}\text{NiO}_3$ catalyst obtained during OSR under $\text{H}_2\text{O}/\text{ethanol}$ molar ratio = 3.0 and $\text{O}_2/\text{ethanol}$ molar ratio = 0.5 at (a) 573 K; (b) 1073 K; (c) $\text{H}_2\text{O}/\text{ethanol}$ molar ratio = 3.0 and $\text{O}_2/\text{ethanol}$ molar ratio = 0.25 at 773 K. (Mass of catalyst = 20 mg and residence time = 0.02 g s/mL.)

and H_2 . These results indicate that oxidative dehydrogenation of ethanol and ethanol combustion are the main reactions that occur at this low temperature. Increasing reaction temperature to 1073 K, ethanol is completely converted to H_2 , CO_2 and CO . Acetaldehyde is no longer detected and only small amount of CH_4 is also observed. In comparison to the reaction at 773 K (Fig. 4c), the selectivity to H_2 is quite similar. However, the selectivity to CO_2 decreased whereas the selectivity to CO increased when the reaction is carried out at high temperature.

In order to investigate the effect of O_2 concentration in the feed for the OSR at 773 K, the $\text{O}_2/\text{ethanol}$ molar ratio was decreased from 0.5 (Fig. 4c) to 0.25 (Fig. 7c). Ethanol conversion slightly decreased from 100% to 90% during 30 h TOS. H_2 , CO_2 and CO were the main products formed. Decreasing the $\text{O}_2/\text{ethanol}$ molar ratio increased the selectivity to H_2 and decreased the selectivity to CO_2 . These results are in agreement with the work of Laosiripojana and Assabumrungrat [38]. They studied the OSR of ethanol over Ni/CeO_2 catalyst under different $\text{O}_2/\text{ethanol}$ molar ratios. Increasing the $\text{O}_2/\text{ethanol}$ molar ratio resulted in a decrease of H_2 selectivity. The addition of high oxygen concentration to the feed favored the combustion of H_2 to H_2O due to the oxidation of Ni particles to NiO . However, higher $\text{O}_2/\text{ethanol}$ molar ratios significantly decreased the formation of carbon.

SEM and TG analyses of the used catalyst were performed to investigate the formation of carbon over $\text{La}_{0.9}\text{Ce}_{0.1}\text{NiO}_3$ catalyst under these reaction conditions. SEM image of the $\text{La}_{0.9}\text{Ce}_{0.1}\text{NiO}_3$ catalyst after OSR at 573 and 1073 K did not show the presence of carbon filaments (Fig. 8a and b), which is in agreement with TG experiments. However, decreasing the $\text{O}_2/\text{ethanol}$ molar ratio to 0.25 led to the appearance of carbon filaments in some regions (Fig. 8c). The amount of carbon determined by TG was 0.7 mg C/g_{cat}/h. This result indicates that an $\text{O}_2/\text{ethanol}$ molar ratio of 0.5 is limit for inhibiting carbon formation at 773 K. For this $\text{O}_2/\text{ethanol}$ molar ratio, carbon formation does not occur regardless of the reaction temperature.

3.3. General discussion

The higher stability of perovskite-type oxides catalysts for reactions like partial oxidation and the CO_2 reforming of methane has been attributed to the highly dispersed metal particles obtained after reduction [29]. The dissociation of methane to H and C requires a defined number of sites (i.e., an ensemble) [39]. Below a critical ensemble size, carbon formation does not take place [40]. Therefore, the higher Ni dispersion obtained from the reduction of perovskite-type oxide materials could decrease or inhibit carbon formation.

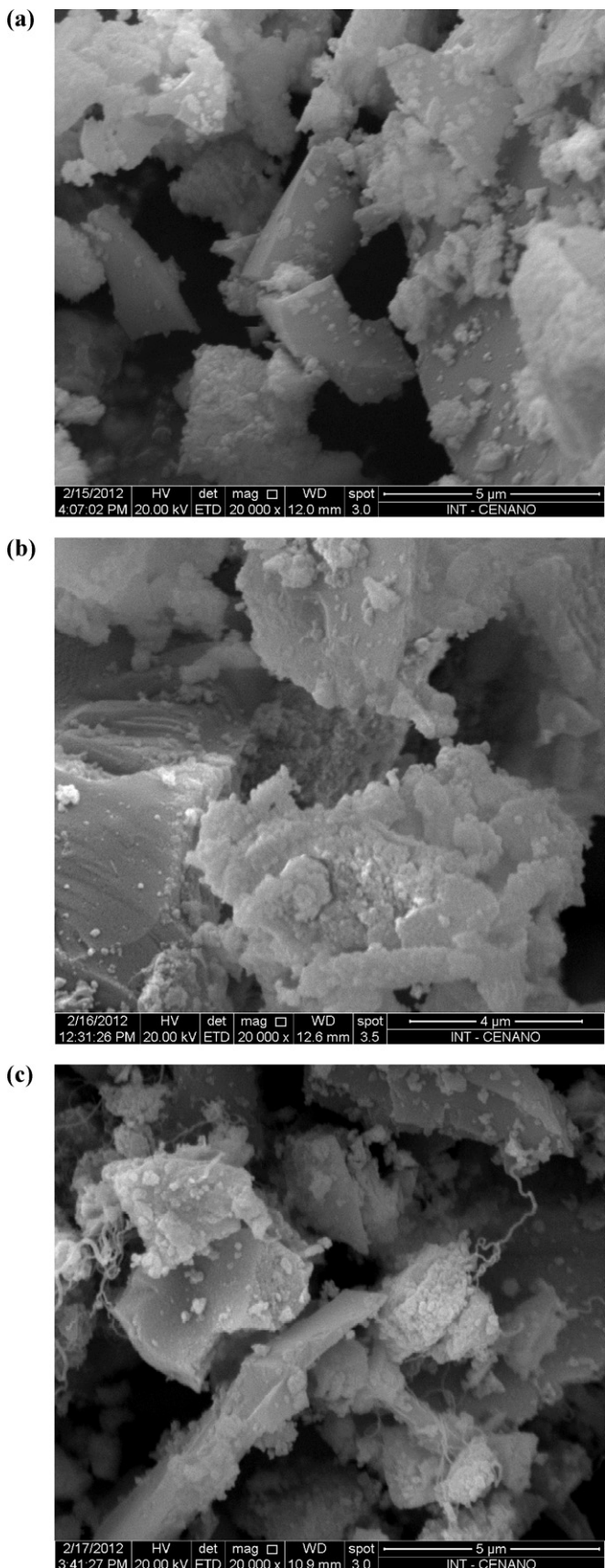


Fig. 8. SEM images after OSR of ethanol over $\text{La}_{0.90}\text{Ce}_{0.10}\text{NiO}_3$ catalyst under $\text{H}_2\text{O}/\text{ethanol}$ molar ratio = 3.0 and $\text{O}_2/\text{ethanol}$ molar ratio = 0.5 at (a) 573 K; (b) 1073 K; (c) $\text{H}_2\text{O}/\text{ethanol}$ molar ratio = 3.0 and $\text{O}_2/\text{ethanol}$ molar ratio = 0.25 at 773 K. (Mass of catalyst = 20 mg and residence time = 0.02 g s/mL.)

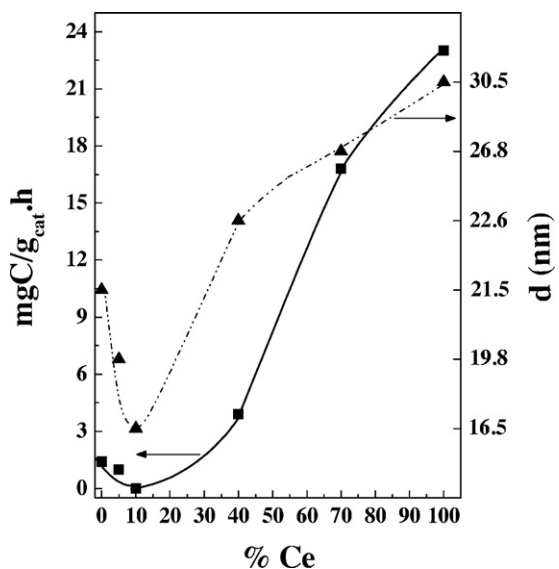


Fig. 9. Amount of carbon formed and Ni crystallite size as a function of Ce content.

However, there are only few reports about the effect of metal particle size on the carbon formation during ethanol conversion reactions. de Lima et al. [28] compared the performance on OSR of a Ni-based catalyst derived from a LaNiO_3 perovskite-type oxide precursor with that of a La_2O_3 supported Ni metal catalyst prepared by the conventional impregnation method of catalyst preparation. The amount of carbon deposited during OSR at 773 K over the $\text{Ni/La}_2\text{O}_3$ catalyst prepared by the conventional method was significantly higher (i.e., 6-fold) than that observed for the $\text{Ni/La}_2\text{O}_3$ catalysts derived from the LaNiO_3 perovskite-type oxide. A higher Ni dispersion obtained through the reduction of LaNiO_3 perovskite-type oxide was postulated to be responsible for the decrease in the carbon formation rate. The same result was observed by Chen et al. [27] for the OSR of ethanol over LaNiO_3 and $\text{Ni/La}_2\text{O}_3$ catalysts. The higher resistance to carbon deposition for the reduced LaNiO_3 was attributed to the highly dispersed Ni particles and the formation of $\text{La}_2\text{O}_2\text{CO}_3$, which strongly interacts with Ni particles, inhibiting sintering during reaction.

In the present work, a clear relationship exists between Ni crystallite size and the amount of carbon deposits (Fig. 9). Carbon formation did not occur on the $\text{La}_{1-x}\text{Ce}_x\text{NiO}_3$ catalyst containing 10% of Ce that exhibited the smallest Ni crystallite size. Increasing the Ni crystallite size favored the deposition of carbon. However, catalyst deactivation is not only determined by the initial Ni crystallite size. In fact, the comparison between Ni crystallite size obtained by XRD of reduced catalysts and TEM images of used catalysts (Fig. 6a and c) revealed pronounced metal sintering for CeNiO_3 (30.5 to 109.2 nm) whereas the Ni crystallite size did not change significantly during reaction over $\text{La}_{0.95}\text{Ce}_{0.05}\text{NiO}_3$ catalyst (19.8 to 21.2 nm). Chen et al. [26] also proposed that the lower carbon formation of reduced $\text{La}_{1-x}\text{Ca}_x\text{Fe}_{0.7}\text{Ni}_{0.3}\text{O}_3$ perovskite-type oxides during OSR of ethanol was due to the decrease of sintering of metallic Ni particles in presence of oxygen.

Furthermore, the support may also play an important role on catalyst stability during ethanol conversion reactions. The diffractograms of reduced samples revealed the presence of a higher amount of oxygen vacancies on the reduced $\text{La}_{0.9}\text{Ce}_{0.1}\text{NiO}_3$ sample, which decreased as Ce content increased. The high oxygen storage capacity and oxygen mobility of this catalyst may improve the stability through the reaction of this highly mobile oxygen with carbon species as soon as it forms, and thus keeping the

metal surface free of carbon, inhibiting deactivation. Frusteri et al. [20] studied the performance of Ni/CeO₂ and Ni/MgO for OSR of ethanol. The lower carbon formation observed for Ni/CeO₂ catalyst was also attributed to the high oxygen storage capacity of ceria that favored the reaction of gasification of carbonaceous residues.

Therefore, the high resistance to carbon deposition exhibited by reduced La_{0.90}Ce_{0.10}NiO₃ catalyst is due to the existence of both an optimal Ni crystallite size as well as high oxygen vacancies concentration. However, this catalyst exhibits a slight deactivation during 30 h of TOS in spite of the absence of carbon deposits. According to the literature [20,38,41,42], adding oxygen to the feed assists in the removal of carbon formed during the reaction. However, one possible side effect is oxidation of the metal particles. This may result in losses in steam reforming activity and H₂ selectivity as well as a higher selectivity to acetaldehyde and CO₂ [42,43]. Therefore, the presence of a metal oxide favors the total oxidation of ethanol to CO₂ and water and the ethanol dehydrogenation to acetaldehyde. da Silva et al. [42] investigated the oxidation of cobalt particles during the OSR of ethanol over Co/CNF catalysts containing different Co loadings. The unreduced samples exhibit a higher selectivity to acetaldehyde and a lower selectivity to hydrogen than the reduced ones. The comparison between the product distribution of unreduced and reduced catalysts suggested that the oxidation of Co particles occurred. This was the main reason for the deactivation of catalyst containing low Co content. Therefore, the partial oxidation of the Ni active sites by oxygen from the feed during OSR over reduced La_{1-x}Ce_xNiO₃ catalysts cannot be ruled out.

4. Conclusions

La_{1-x}Ce_xNiO₃ perovskite-type oxide precursor ($x=0, 0.05, 0.1, 0.4, 0.7$ and 1.0) is prepared by amorphous citrate decomposition method. The LaNiO₃ structure is the only phase formed for $x=0$. The incorporation of Ce led to the segregation of different phases: La₂NiO₄, CeO₂ and NiO. The reduction of La_{1-x}Ce_xNiO₃ perovskite-type oxide led to the formation of La₂O₃ or CeO_x-supported Ni⁰ particles. LaNiO₃ and La_{0.95}Ce_{0.05}NiO₃ catalysts consisted of Ni⁰ particles deposited over La₂O₃. Above $x=0.1$, the reduced samples were composed of Ni/CeO_x and the oxygen vacancies of ceria depended on the ceria content. The reduced La_{0.9}Ce_{0.1}NiO₃ sample contained mainly Ce₂O₃ whereas CeNiO₃ is formed by CeO₂.

All catalysts are active and selective to hydrogen but carbon deposition occurred except for La_{0.90}Ce_{0.10}NiO₃. The partial substitution of La³⁺ cations by Ce³⁺ cations improved the resistance to carbon deposition. It is found that the amount of carbon formed on the different catalysts after 30 h of TOS went through a minimum as a function of Ce content in the support and the minimum occurred at the composition that exhibited both the smallest Ni crystallite size and the highest concentration of oxygen vacancies. The high OSC and oxygen mobility of La_{0.90}Ce_{0.10}NiO₃ catalyst also improved the resistance to carbon formation. This highly mobile oxygen reacts with carbon species as soon as it forms, and thus keeping the metal surface free of carbon, inhibiting deactivation. Therefore, La_{0.90}Ce_{0.10}NiO₃ catalyst developed in our work is able to carry out the OSR of ethanol without any formation of carbon by using an O₂/ethanol molar ratio of 0.5 and reaction temperature range of 573–1073 K, which is a very promising catalyst for hydrogen production.

Acknowledgment

This work received financial support of CNPq (CT-INFO/CT-HIDRO/MCT/CNPq – 490818/2007-2).

References

- [1] A. Haryanto, S. Fernando, N. Murali, S. Adhikari, Energy and Fuels 19 (2005) 2098–2106.
- [2] P.D. Vaidya, A.E. Rodrigues, Chemical Engineering Journal 117 (2006) 39–49.
- [3] M. Ni, Y.C. Leung, M.K.H. Leung, International Journal of Hydrogen Energy 32 (2007) 3238–3247.
- [4] P.R. de la Piscina, N. Homs, Chemical Society Reviews 37 (2008) 2459–2467.
- [5] A.N. Fatsikostas, X.E. Verykios, Journal of Catalysis 225 (2004) 439–452.
- [6] J. Llorca, P.R. de la Piscina, J. Sales, N. Homs, Chemical Communications (2001) 641–642.
- [7] J.W.C. Liberatori, R.U. Ribeiro, D. Zanchet, F.B. Noronha, J.M.C. Bueno, Applied Catalysis A 327 (2007) 197–204.
- [8] V. Fierro, O. Akdim, C. Mirodatos, Green Chemistry 5 (2003) 20–24.
- [9] H. Song, U.S. Ozkan, Journal of Catalysis 261 (2009) 66–74.
- [10] T. Nishiguchi, T. Matsumoto, H. Kanai, K. Utani, Y. Matsumura, W.J. Shen, S. Imaamura, Applied Catalysis A 279 (2005) 273–277.
- [11] D.K. Liguras, D.I. Kondarides, X.E. Verykios, Applied Catalysis B 43 (2003) 345–354.
- [12] M. Domok, M. Tóth, J. Raskó, A. Erdohelyi, Applied Catalysis B 69 (2007) 262–272.
- [13] L.V. Mattos, F.B. Noronha, Journal of Catalysis 233 (2005) 453–463.
- [14] F. Aupretre, C. Descorne, D. Duprez, Catalysis Communications 3 (2002) 263–267.
- [15] S.M. de Lima, A.M. da Silva, U.M. Graham, G. Jacobs, B.H. Davis, L.V. Mattos, F.B. Noronha, Applied Catalysis A 352 (2009) 95–113.
- [16] A. Erdohelyi, J. Raskó, T. Kecskés, M. Tóth, M. Dömök, K. Baán, Catalysis Today 116 (2006) 367–376.
- [17] H. Roh, A. Platon, Y. Wang, D.L. King, Catalysis Letters 110 (2006) 1–6.
- [18] W. Cai, F. Wang, E. Zhan, A.C. van Veen, C. Mirodatos, W. Shen, Journal of Catalysis 257 (2008) 96–107.
- [19] S. Cavallaro, N. Mondelo, S. Freni, Journal of Power Sources 102 (2001) 198–204.
- [20] F. Frusteri, S. Freni, V. Chiodo, S. Donato, G. Bonura, S. Cavallaro, International Journal of Hydrogen Energy 31 (2006) 2193–2199.
- [21] G. Valderrama, M.R. Goldwasser, C.U. de Navarro, J.M. Tatibouë, J. Barrault, C. Batiot-Dupeyrat, F. Martínez, Catalysis Today 107 (2005) 785–791.
- [22] S.M. de Lima, A.M. da Silva, L.O.O. da Costa, G. Jacobs, B.H. Davis, L.V. Mattos, F.B. Noronha, Journal of Catalysis 268 (2009) 268–281.
- [23] K. Urasaki, K. Tokunaga, Y. Sekine, M. Matsukata, E. Kikuchi, Catalysis Communications 9 (2008) 600–604.
- [24] M.M. Natile, F. Poletto, A. Galenda, A. Glisenti, T. Montini, L. De Rogatis, P. Fornasiero, Chemistry of Materials 20 (2008) 2314–2327.
- [25] J.Y. Liu, C.C. Lee, C.H. Wang, C.T. Yeh, C.B. Wang, International Journal of Hydrogen Energy 35 (2010) 4069–4075.
- [26] S.Q. Chen, Y.D. Liu, Y. Liu, X. Bai, International Journal of Hydrogen Energy 36 (2011) 5849–5856.
- [27] H. Chen, H. Yu, F. Peng, G. Yang, H. Wang, J. Yang, Y. Tang, Chemical Engineering Journal 160 (2010) 333–339.
- [28] S.M. de Lima, A.M. da Silva, L.O.O. da Costa, J.M. Assaf, G. Jacobs, B.H. Davis, L.V. Mattos, F.B. Noronha, Applied Catalysis A 377 (2010) 181–190.
- [29] M.A. Peña, J.L.G. Fierro, Chemical Reviews 101 (2001) 1981–2017.
- [30] S.M. Lima, J.M. Assaf, M.A. Peña, J.L.G. Fierro, Applied Catalysis A 311 (2006) 94–104.
- [31] D. Ferri, L. Forni, Applied Catalysis B 16 (1998) 119–126.
- [32] M. Ghasdi, H. Almardaria, S. Royer, A. Adnot, Sensors and Actuators B 156 (2011) 147–155.
- [33] F.B. Passos, E.R. de Oliveira, L.V. Mattos, F.B. Noronha, Catalysis Today 101 (2005) 23–30.
- [34] N. Hirosaki, S. Ogata, C. Kocer, Journal of Alloys and Compounds 351 (2003) 31–34.
- [35] E.A. Kummerle, G. Heger, Journal of Solid State Chemistry 147 (1999) 485–500.
- [36] A.E. Galetti, M.F. Gomez, L.A. Arrúa, M.C. Abello, Applied Catalysis A 348 (2008) 94–102.
- [37] M.C. Sánchez-Sánchez, R.M. Navarro, J.L.G. Fierro, International Journal of Hydrogen Energy 32 (2007) 1462–1471.
- [38] N. Laosiripojana, S. Assabumrungrat, Applied Catalysis A 327 (2007) 180–188.
- [39] D.L. Trimm, Catalysis Today 37 (1997) 233–238.
- [40] J.R. Rostrup-Nielsen, Journal of Catalysis 85 (1984) 31–43.
- [41] J. Kugai, S. Velu, C. Song, M.H. Engelhard, Y. Chin, Journal of Catalysis 238 (2006) 430–440.
- [42] A.L.M. da Silva, L.V. Mattos, J.P. den Breejen, J.H. Bitter, K.P. de Jong, F.B. Noronha, Catalysis Today 164 (2011) 262–267.
- [43] E.B. Pereira, N. Homs, S. Martí, J.L.G. Fierro, P.R. de la Piscina, Journal of Catalysis 257 (2008) 206–214.